Journal of Energy Chemistry 54 (2021) 815–821

Contents lists available at ScienceDirect

Journal of Energy Chemistry

journal homepage: www.elsevier.com/locate/jechem

http://www.journals.elsevier.com/journal-of-energy-chemistry/

Switching O—O bond formation mechanism between WNA and I2M pathways by modifying the Ru-bda backbone ligands of water-oxidation catalysts

Biaobiao Zhang [a,*,1], Shaoqi Zhan [b,1], Tianqi Liu [a], Linqin Wang [a], A. Ken Inge [c], Lele Duan [d], Brian J.J. Timmer [a], Oleksandr Kravchenko [a], Fei Li [e], Mårten S.G. Ahlquist [b,*], Licheng Sun [a,e]

[a] Department of Chemistry, KTH Royal Institute of Technology, 10044 Stockholm, Sweden
[b] Department of Theoretical Chemistry & Biology, School of Engineering Sciences in Chemistry Biotechnology and Health, KTH Royal Institute of Technology, 10691 Stockholm, Sweden
[c] Department of Materials and Environmental Chemistry, Stockholm University, 10691 Stockholm, Sweden
[d] Department of Chemistry, Southern University of Science and Technology (SUSTech), Shenzhen 518055, Guangdong, China
[e] State Key Laboratory of Fine Chemicals, Institute of Artificial Photosynthesis, DUT–KTH Joint Education and Research Center on Molecular Devices, Dalian University of Technology (DUT), Dalian 116024, Liaoning, China

ARTICLE INFO

Article history:
Received 19 February 2020
Revised 10 June 2020
Accepted 11 June 2020
Available online 26 June 2020

Keywords:
Water oxidation
Oxygen evolution
Ruthenium
O—O bond formation

ABSTRACT

Understanding the seven coordination and O—O coupling pathway of the distinguished Ru-bda catalysts is essential for the development of next generation efficient water-oxidation catalysts based on earth-abundant metals. This work reports the synthesis, characterization and catalytic properties of a monomeric ruthenium catalyst Ru-bnda (H_2bnda = 2,2′-bi(nicotinic acid)-6,6′-dicarboxylic acid) featuring steric hindrance and enhanced hydrophilicity on the backbone. Combining experimental evidence with systematic density functional theory calculations on the Ru-bnda and related catalysts Ru-bda (H_2bda = 2,2′-bipyridine-6,6′-dicarboxylic acid), Ru-pda (H_2pda = 1,10-phenanthroline-2,9-dicarboxylic acid), and Ru-biqa (H_2biqa = (1,1′-biisoquinoline)-3,3′-dicarboxylic acid), we emphasized that seven coordination clearly determines presence of Ru^V=O with high spin density on the $O_{RuV=O}$ atom, i.e. oxo with radical properties, which is one of the necessary conditions for reacting through the O—O coupling pathway. However, an additional factor to make the condition sufficient is the favorable intermolecular face-to-face interaction for the generation of the pre-reactive [Ru^V=O···O=Ru^V], which may be significantly influenced by the secondary coordination environments. This work provides a new understanding of the structure–activity relationship of water-oxidation catalysts and their potential to adopt I2M pathway for O—O bond formation.

© 2020 The Authors. Published by ELSEVIER B.V. and Science Press on behalf of Science Press and Dalian Institute of Chemical Physics, Chinese Academy of Sciences. This is an open access article under the CC BY-NC-ND license (http://creativecommons.org/licenses/by-nc-nd/4.0/).

1. Introduction

The increasing negative ecological impact and looming energy crisis make artificial photosynthetic schemes for the storage of solar energy into fuels, such as H_2 and hydrocarbons via reduction of proton and CO_2 respectively, more and more attractive.[1] However, a major bottleneck of artificial photosynthesis is water oxidation ($2H_2O \rightarrow O_2 + 4e^- + 4H^+$, E_0 = 1.23 V *vs* NHE at pH = 0, NHE = Normal Hydrogen Electrode), which is considered the ideal way to provide abundant electrons and protons for the reduction reactions [1]. Molecular catalysts provide a promising entry to intrinsically efficient water oxidation catalysts with low overpotential, because both the steric and electronic structures of molecular catalysts can be precisely adjusted, guided by deep understanding of the catalytic mechanism, which is especially accessible for molecular catalysts [2,3].

Among numerous molecular water-oxidation catalysts (WOCs) developed in recent years [4–10], the most efficient ones to date belong to the Ru-bda family of catalysts [Ru^{II}(bda)$(L)_2$], which comprises a tetradentate bipyridyl-dicarboxylate bda (H_2bda = 2,2′-bi pyridine-6,6′-dicarboxylic acid) as equatorial ligand and two aromatic *N*-heterocycles as axial ligands L (Fig. 1) [11–15]. Kinetic and density functional theory (DFT) studies indicated that O—O bond formation with Ru-bda catalysts takes place by interaction of two metal-oxo units (*i.e.* I2M pathway) [15–17]. The overpotential required by Ru-bda catalyst for water oxidation is lower than

* Corresponding authors.
E-mail addresses: biaobiao@kth.se (B. Zhang), ahlqui@kth.se (M.S.G. Ahlquist).
[1] These authors contributed equally to this work.

https://doi.org/10.1016/j.jechem.2020.06.036
2095-4956/© 2020 The Authors. Published by ELSEVIER B.V. and Science Press on behalf of Science Press and Dalian Institute of Chemical Physics, Chinese Academy of Sciences. This is an open access article under the CC BY-NC-ND license (http://creativecommons.org/licenses/by-nc-nd/4.0/).

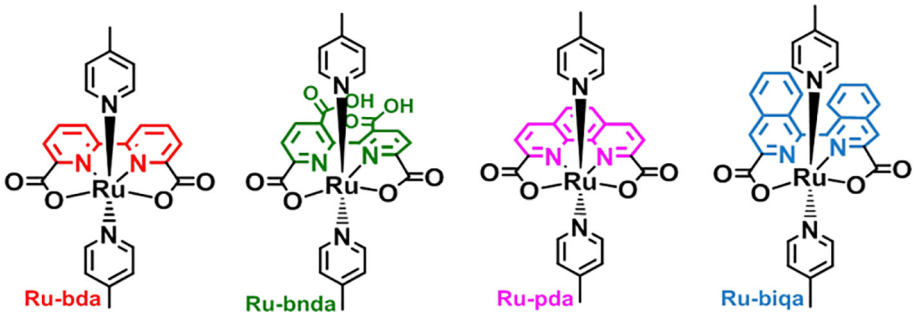


Fig. 1. Structures of the parent Ru(bda)(pic)$_2$ catalyst and its derivatives Ru(bnda)(pic)$_2$, Ru(pda)(pic)$_2$, and Ru(biqa)(pic)$_2$ (H_2biqa = (1,1′-biisoquinoline)-3,3′-dicarboxylic acid).

200 mV, close to that of the natural oxygen-evolving complex (OEC) in photosystem II (~160 mV) [14,15,17]. With using Ce^{IV} ($(NH_4)_2[Ce(NO_3)_6]$) as the oxidant, a catalytic turnover frequency (TOF) of Ru-bda catalysts comparable to the TOF of the in vivo OEC can be achieved [14,15,17]. WOCs with excellent catalytic performances have finally been obtained after thirty-years research; unfortunately, they are based on Ru which is a noble metal and ought to be replaced. To enlighten development of efficient earth-abundant metal based WOCs [18–24], further investigation of the coordination environment of the Ru-bda catalysts is thus in high demand to understand the real reasons behind their outstanding performance and unique I2M mechanism.

Both the equatorial bda ligand and two axial ligands of Ru-bda catalysts play an essential role in establishing the catalytic activity [25,26]. The facile manipulation of the axial ligands allowed for studies on dozens of different Ru-bda catalysts to reveal the effects of axial ligands on catalysis, such as the electronic effect, π-π stacking and other non-covalent effects [15,27-30]. Nevertheless, the adjustments of axial ligands in most of cases influenced only the rate of catalytic water oxidation, and did not lead to deviation from the I2M mechanism, which comprises the most unique feature of Ru-bda catalysts and is responsible for the high activity.

To fundamentally understand the outstanding activity of Ru-bda catalysts for water oxidation, it is necessary to investigate the bda backbone in more detail by designing closely related analogues. However, reports on modified bda ligands are rare, due to the synthetic challenge of introducing substituents. Gao et al. and Concepcion et al. researched the electronic effect by introduction of —Br and —CF_3 substituents to the bda backbone, respectively [31,32]. Replacing the equatorial ligand bda with other polypyridyl backbone ligands containing carboxylates, e.g. pdc (H_2pdc = 2,6-pyridinedicarboxylic acid) [33,34], pda (H_2pda = 1,10-phenanthroline-2,9-dicarboxylic acid) [35] and tda (H_2tda = (2,2′:6′,2″-terpyridine)-6,6″-dicarboxylic acid) [36–38], switches the O—O bond formation pathway from I2M to water nucleophilic attack (WNA), the pathway commonly observed for polypyridyl ruthenium catalysts [4,39–41]. Effects of replacing the carboxylate groups with phosphonate groups has been independently reported by the Grotjahn and Concepcion groups [42–44]. Recently, the Duan group replaced the bda ligand with a 2,2′-bipyridine-6,6′-dicarbothioate (bct) ligand and studied a mononuclear Ru-bda analogue, the Ru(bct)(pic)$_2$, which was found to be transformed into the Ru(bda)(pic)$_2$ during electrochemical and chemical oxidation [45]. In addition, effects of the coordination numbers and charge of the Ru^V=O species on the pathway of O—O bond formation have been disclosed by displacing one of the carboxylate for a pyridyl [46]. Catalytic performance and catalytic mechanism variations of Ru-bda based catalysts have also been studied within supramolecular systems [47,48].

Based on these results it is apparent that the mechanistic distinction is dominated by the unique configuration and coordination environment in the equatorial plane of the Ru-bda catalysts. Herein, we investigate the influence of steric hindrance and hydrophilicity character of the bda backbone by substituting the 3,3′-positions with two sterically hindered carboxyl groups, reporting a monomeric ruthenium catalyst Ru(bnda)(pic)$_2$ (Ru-bnda, H_2bnda = 2,2′-bi(nicotinic acid)-6,6′-dicarboxylic acid, pic = 4-picoline). Mechanistic insights on water oxidation catalyzed by the Ru-bnda under acidic conditions were revealed by the observed electrochemistry, time-resolved ESI-HRMS as well as O_2-evolution kinetic studies, and were further rationalized by DFT calculations.

2. Experimental

2.1. Materials and synthesis

The *cis*-Ru(DMSO)$_4$Cl$_2$ was prepared according to previously published methods [49]. 70% HNO_3 (99.999% purity), $(NH_4)_2[Ce^{IV}(NO_3)_6]$, other reagents and solvents were purchased from Sigma-Aldrich and used without further purification unless noted otherwise. Ultra pure water (18.2 MΩ·cm^{-1}) for all the reactions or measurements was obtained from a Milli-Q purification system.

Synthesis of the H_2bnda ligand [50]. 2.08 g (10 mmol) of 2,9-dimethyl-1,10-phenanthroline, 0.80 g (20 mmol) of NaOH and 10 g (63.30 mmol) of $KMnO_4$ were mixed in 75 mL of water. The mixture was refluxed for 8 h and the precipitate was filtered off. The filtrate was then treated with activated carbon and concentrated to 40 mL. The obtained solution was acidified to pH 1.5 with concentrated hydrochloric acid. The formed white product was recrystallized from water (yield: 2.35 g, 71%). ^{1}H NMR (400 MHz, D_2O): 8.20 (d, 2H, J = 8 Hz), 8.50 (d, 2H, J = 8 Hz). HRMS: m/z = 330.9815 [M−H]$^-$, calcd. for $C_{14}H_7N_2O_8$ 331.0202. Found: C, 50.2; H, 2.8; N 8.2. Calcd. for $C_{14}H_8N_2O_8$: C, 50.6; H, 2.4; N, 8.4.

*Synthesis of Ru-bnda (**1**).* A mixture of *cis*-Ru(DMSO)$_4$Cl$_2$ (194 mg, 0.4 mmol), H_2bnda (133 mg, 0.4 mmol), and triethylamine (300 μL) was refluxed in methanol (15 mL) overnight under N_2 atmosphere. An excess of 4-methylpyridine (1 mL) was added, and the solution was refluxed for another 5 h. The solvent was removed. The crude product was purified by silica gel column chromatography using MeOH/CH_2Cl_2 (v/v 1:10) as eluent to isolate the complex Ru-bnda (79 mg, 32%). Two drops of acetic acid were added to the eluent to protonate the carboxyl groups of the catalyst backbone. ^{1}H NMR (400 MHz, D_2O): 2.22 (s, 6H), 7.03 (d, 4H, J = 8 Hz), 7.61 (d, 4H, J = 8 Hz), 8.02 (m, 4H). ^{13}C NMR (101 MHz, D_2O): 19.51, 125.27, 125.71, 132.20, 143.43, 149.29, 151.21, 153.71, 160.29, 170.14, 174.77. HRMS: m/z = 619.0393 [M+H]$^+$, calcd. for $C_{26}H_{20}N_4O_8Ru$ 619.0403. Found: C, 50.3; H, 3.6; N 8.9. Calcd. for $C_{26}H_{20}N_4O_8Ru$: C, 50.6; H, 3.3; N, 9.1.

2.2. Physical methods

The NMR spectra were recorded with 400 MHz Bruker Avance spectrometer. Mass spectrometry was measured on a Q-Tof Micromass spectrometer (Manchester, England). *Ex-situ* mass spectrometry measurements to capture the Ru^{III} and Ru^{IV} intermediates were carried out by using an LTQ-Orbitrap XL Micromass spectrometer (Thermo Scientific, USA). Electrochemical measurements were performed with a CHI 650e potentiostat. The cell was equipped with a glassy carbon disk (ϕ = 3 mm) as the working electrode, a platinum wire as the counter electrode, and an Ag/AgCl (3 M) electrode as the reference electrode. Potentials *vs.* NHE were determined by adding +0.197 V to the potentials measured versus Ag/AgCl (3 M) electrode. Oxygen evolution curves were recorded by a pressure sensor and calibrated with the actual quantity of O_2 as determined by gas chromatography (Shimadzu, Model GC-2014). The detailed experimental procedures are available in our previous reports [11]. The bulk electrolytic experiments of the Ru-bnda solution were carried out in a H-type two chamber cell under helium atmosphere with Pt mesh as counter electrode and carbon foam or a large Pt mesh as working electrode. For the Faradaic efficiency detection, the amount of oxygen evolution during electrolysis at 1.6 V was quantified by GC-2014.

Crystals of Ru-bnda suitable for single crystal X-ray diffraction were obtained by slowly evaporating acetic acid into an aqueous solution of Ru-bnda. The diffraction data were measured using Mo Kα radiation on a Bruker D8 VENTURE single crystal X-ray diffractometer equipped with a PHOTON II CPAD detector and kappa geometry goniometer. The crystal was kept at 100 K during data collection. The crystal structure was solved and refined by SHELXT and SHELXL respectively [51]. All the non-hydrogen atoms were refined with anisotropic displacement parameters. The positions of all hydrogen atoms were determined upon examination of difference Fourier maps and their isotropic displacement parameters were fixed with respect to the parent carbon or oxygen atom. Details of crystal data (CCDC 1884248), data collection and structure refinements are summarized in Tables S1 and S2. These data can be obtained free from the Cambridge Crystallographic Data Centre via www.ccdc.cam.ac.uk/data_request/cif.

2.3. Theoretical study

All DFT calculations for the estimation of Gibbs free energies were carried out with the Jaguar 8.3 program package by Schrödinger LLC [52]. Molecular geometries were optimized using Becke's three-parameter hybrid functional and the LYP correlation functional (B3LYP) [53] with D3 correction of Grimme et al. [54,55] and the LACVP** basis set [56]. Single-point energy corrections were performed with the B3LYP-D3 functional using LACV3P**++ basis set augmented with two f-functions on the metal. To identify the transition states of I2M mechanism, we probed the potential energy surface by scanning the terminal O-O bond distance [Ru^{V}=O···O=Ru^{V}] of the antiferromagnetic open shell singlet. To identify the transition states of WNA mechanism, two additional water molecules were included. Frequency calculations were performed on the optimized geometries to verify that the geometries correspond to minima or first-order saddle points (transition states) on the potential energy surface (PES). On the basis of the gas phase optimized geometries, the solvation energies were estimated by the single-point calculations using the Poisson–Boltzmann reactive field implemented in Jaguar 8.3 (PBF) in water. The Gibbs free energy was defined by the following equation G = E(B3LYP-D3/LACV3P**++ 2f on Ru) + G_{sol} + ZPE + H_{298} – TS_{298} + 1.9 kcal/mol (a value being a concentration correction to the free energy of solvation which by default is calculated at 1 M (g) to 1 M (aq) in Jaguar).

3. Results

The H_2bnda ligand was readily obtained by one step oxidation of the commercially available 2,9-dimethyl-1,10-phenanthroline and subsequent acidification (Figs. S1–S3) [50]. Ru-bnda was then prepared by a two-step one-pot procedure according to the synthesis of Ru-bda complex (Fig. S1). The obtained Ru-bnda was characterized by ^{1}H NMR (Nuclear Magnetic Resonance), ^{13}C NMR and HR ESI-MS (High Resolution Electrospray Ionization Mass Spectrometry) (Figs. S4–S6). The ^{1}H NMR spectrum of Ru-bnda agrees with a C_{2v} symmetrical structure of the complex under NMR conditions. The formation of Ru-bnda was further confirmed by HRMS (m/z: $[M+H]^+$ calcd. for 619.0403; found 619.0393). The UV/Vis spectrum of Ru-bnda shows metal-to-ligand charge transfer (MLCT) transition bands at 430 nm (shoulder) and 540 nm (shoulder), and strong π–π* transition absorptions originated from the ligands between 200 nm and 350 nm (Fig. S7).

The steric conformation of the Ru-bnda was revealed by X-ray diffraction analysis on a single crystal obtained from acidic aqueous solution (Table S1, Table S2 and Fig. 2). In general, Ru-bnda presents a very similar primary coordination sphere as Ru-bda. The inherent twist introduced by two sterically hindered carboxyl groups in the H_2bnda ligand leads to no obvious distortion of the equatorial coordination geometry of Ru-bnda. The O1—Ru1—O2 angle of 116.36° is still much larger than the ideal 90° of an octahedral configuration, although it is smaller than the 122.99° and 130.5° observed for Ru-bda and Ru-pda, respectively. However, as expected, there are distinct differences in the the secondary coordination spheres of Ru-bnda. The two hindered carboxyl groups are clearly bent, and the two pyridine rings in the bnda plane are slightly bent with a dihedral angle of 18.3° (Fig. 2), introducing strain in the equatorial coordination to the ruthenium center. Moreover, the introduced hydrophilicity on the back of the Ru-bnda is readily observable in the crystal packing structure of Ru-bnda, where the Ru-bnda molecules are packing back to back with hydrogen bonds between carboxyl groups and carboxylate groups on neighboring complexes, and also with water molecules in between complexes which also form hydrogen bonds with the carboxylate groups (Fig. 2).

Electrochemical behavior of Ru-bnda was studied by cyclic voltammetry (CV) and differential pulse voltammetry (DPV) in a 0.1 M CF_3SO_3H aqueous solution mixed with 30% 2,2,2-trifluoroethanol (TFE), which is used to enhance solubility of Ru-bnda. A redox peak at 0.73 V was obviously visible in the CVs of Ru-bnda (Fig. S8a) at scan rate of 0.1 V s^{-1}. Further oxidation steps and a distinct catalytic peak can be observed in the CV at low scan rate (Fig. 3). Two weak oxidation peaks near by the water-oxidation peak were displayed in the DPV of Ru-bnda at 1.04 V and 1.29 V (Fig. 3). The first oxidation peak at 0.73 V was assigned to the Ru^{II}/Ru^{III} couple according to the bulk electrolysis experiment, where it clearly indicated a one-electron oxidation (Fig. S8b). The following two peaks at 1.04 V and 1.29 V can be respectively attributed to the Ru^{III}/Ru^{IV} and Ru^{IV}/Ru^{V} couples [11]. Compared with the parent Ru(bda)(pic)$_2$, the Ru^{II}/Ru^{III} redox potential of 1 is over 100 mV higher due to the effect of the two back carboxyl groups, while Ru^{III}/Ru^{IV} and Ru^{IV}/Ru^{V} redox potentials are similar to those of the Ru(bda)(pic)$_2$, indicating the negligible effect of two back carboxyl substituents on the Ru^{III} → Ru^{IV} and Ru^{IV} → Ru^{V} steps [11]. A more detailed comparison of the electrochemical properties of the parent Ru-bda, Ru-bnda, Ru-pda, and Ru-biqa catalysts is provided in Table 1 and discussions below.

The catalytic activity of Ru-bnda was evaluated in 0.1 M CF_3SO_3H containing a large excess of ceric ammonium nitrate (Ce^{IV}) as oxidant. Because the solubility of 1 is worse than the parent Ru(bda)(pic)$_2$ in the acidic solution, a large amount of TFE co-solvent is required to prepare the stock solution of 1 for the

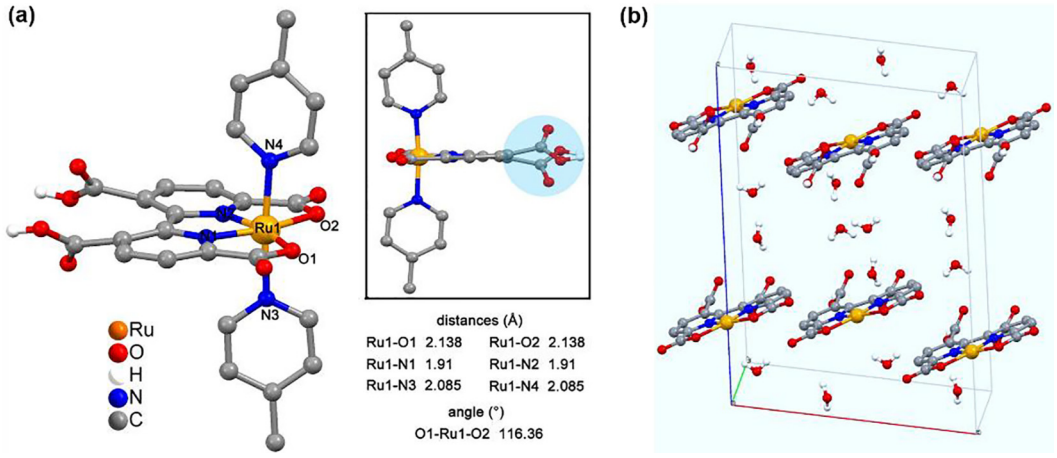


Fig. 2. (a) Crystal structure of Ru(bnda)(pic)$_2$ determined by single crystal X-ray diffraction. Inset shows the planar equatorial coordination geometry and the bending of two sterically hindered carboxyl groups. Solvent molecules and most hydrogen atoms are omitted for clarity. (b) Packing of Ru(bnda)(pic)$_2$ in the crystal. The picoline axial ligands and some hydrogen atoms on the complex are omitted for clarity.

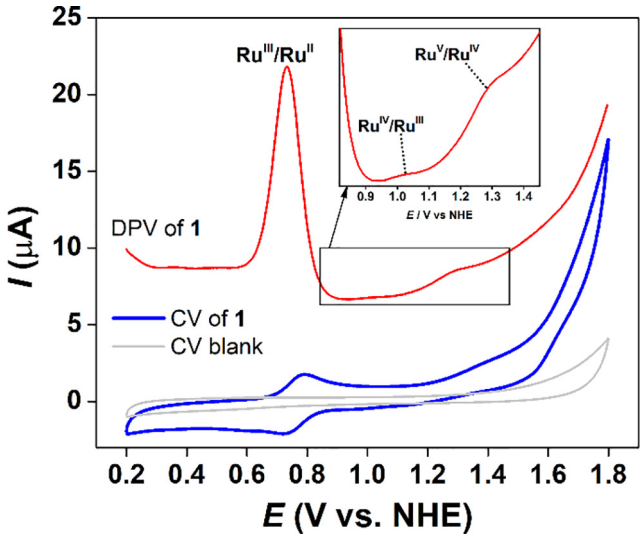


Fig. 3. CV and DPV of Ru-bnda (1) in a 0.1 M CF_3SO_3H aqueous solution mixed with 30% TFE. Working electrode is a glassy carbon electrode. Scan rate of CV is 10 mV/s. For DPV scan, amplitude is 50 mV, pulse width is 50 ms, and pulse period is 0.5 s. Current scale is not applicable for the DPV curve.

oxygen evolution test. The oxygen evolution plot was monitored by a pressure sensor and the amount of oxygen produced was calibrated by gas chromatography. A total TON of 480 was obtained for Ru-bnda within 3 min (Fig. S9). The initial TOF of 10 s^{-1} was obtained from the curve of oxygen evolution in the first 30 s. TOF achieved for the Ru(bda)(pic)$_2$ is 19 s^{-1} under comparable conditions, indicative of similar catalysis rates for both complexes [11]. The kinetics of catalytic water oxidation by Ru-bnda was further investigated via monitoring the initial rate of oxygen evolution (over 0–30 s) at various concentrations of Ce^{IV} and Ru-bnda (Fig. 4). The kinetic results revealed that water oxidation catalyzed by 1 is zero-order in Ce^{IV} (Fig. S10) and second-order in Ru-bnda catalyst with a reaction rate law: rate = 309.8 $mmol^{-1}$ s^{-1} L^2 × [**1**]^2, and a deduced rate constant of 309.8 $mmol^{-1}$ s^{-1} L^2 × [**1**]. It indicates that a binuclear catalytic process is involved in the rate-determining step of water oxidation catalyzed by the Ru-bnda, the same as the I2M mechanism adopted by the parent Ru(bda)(pic)$_2$ catalyst.

To further investigate the catalytic mechanism, HR ESI-MS was employed to track the intermediates involved in the catalytic water oxidation by Ru-bnda. To probe the various intermediate oxidation states, 1, 2, 3 and 8 equivalents of Ce^{IV} were added to different 1.0 mM solutions of Ru-bnda in 0.1 M CF_3SO_3H under fast stirring. The resulting oxidized mixtures were immediately injected into the HR ESI-MS instrument. Fig. S11 shows the mass spectra of Ru-bnda after slow addition of 1, 2, 3 and 8 equivalents of Ce^{IV} to Ru-bnda solutions. For the [Ru^{II}(bnda)(pic)$_2$] complex, the observed main MS peak is 619.0393 ($C_{26}H_{20}N_4O_8Ru$ + H^+, calcd. m/z = 619.0403), indicating the Ru^{II} oxidation state (Fig. S6). After addition of 1 equivalent of Ce^{IV} to a solution of Ru-bnda, the mass spectrum showed a salient cluster at m/z = 618.0334, which is the molecular ion peak of the [Ru^{III}(bnda)(pic)$_2$]$^+$ ($C_{26}H_{20}N_4O_8Ru$, calcd. m/z = 618.0325) species, produced by one-electron oxidation of the

Table 1
Comparisons between the parent Ru-bda, Ru-bnda, Ru-pda, and Ru-biqa catalysts in redox potentials, TONs, TOFs and O—O bond formation pathways.

Catalysts	$E_{1/2}$ (V)			TONs[a]	TOFs (s^{-1})[b]	O—O formation pathways
	Ru$^{II/III}$	Ru$^{III/IV}$	Ru$^{IV/V}$			
Ru-bda [11]	0.60[c]	1.07[c]	1.25[c]	2010	19	I2M
Ru-bnda	0.73[d]	1.04[d]	1.29	480	10	I2M
Ru-pda [35]	0.97[e]	1.36[e]	–	310	0.1	WNA
Ru-biqa [59]	0.67[f]	1.11[f]	1.30[f]	87	0.63	WNA

[a] TONs = moles of produced O_2 per mole of catalyst by using Ce^{IV} oxidant.
[b] TOFs = moles of produced O_2 per mole of catalyst per second by using Ce^{IV} oxidant.
[c] 0.1 M CF_3SO_3H aqueous solution mixed with 25% acetone.
[d] 0.1 M CF_3SO_3H aqueous solution mixed with 30% TFE.
[e] 0.1 M CF_3SO_3H aqueous solution mixed with 10% acetonitrile.
[f] 0.1 M CF_3SO_3H aqueous solution mixed with 20% TFE. More details about experimental conditions can be found in the references.

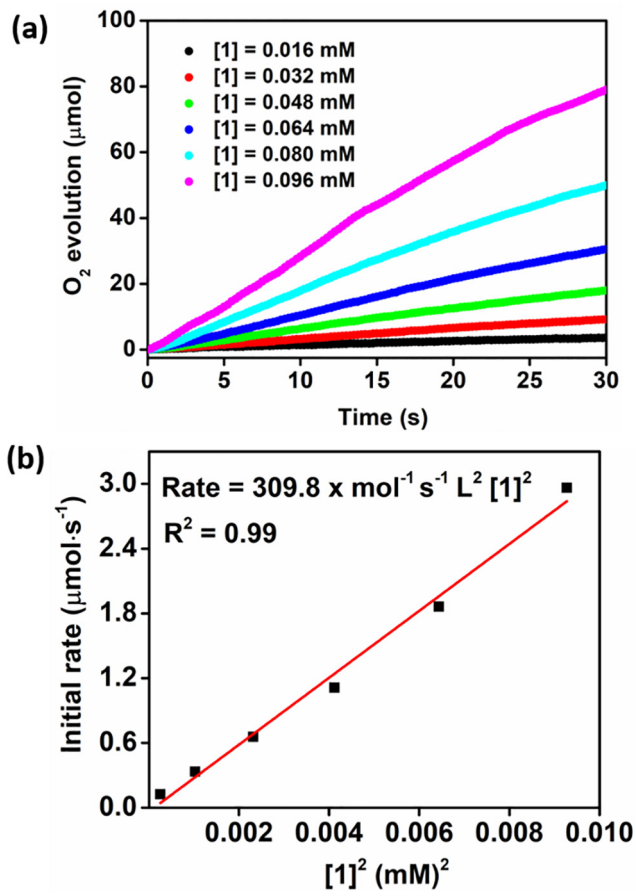


Fig. 4. (a) Oxygen-evolution plots at various concentrations of Ru-bnda (**1**): 0.016 mM, 0.032 mM, 0.048 mM, 0.064 mM, 0.080 mM and 0.096 mM. (b) Plot of initial rate of oxygen evolution *vs.* [Ru-bnda]^2. [Ce^{IV}] = 0.2 M, and V = 3 mL, 0.1 M CF_3SO_3H.

initial $Ru^{II}(bnda)(pic)_2$ catalyst. For the addition of 2 equivalents of Ce^{IV} to the solution of Ru-bnda, the mass spectrum of Ru-bnda, as expected, revealed another distinct mass-to-charge signal at 635.0348, which can be assigned to the $[Ru^{IV}(bnda)(pic)_2(OH)]^+$ ($C_{26}H_{21}N_4O_9Ru$, calcd. m/z = 635.0352) intermediate species. No new species other than the $[Ru^{III}(bnda)(pic)_2]^+$ and $[Ru^{IV}(bnda)(pic)_2(OH)]^+$ were observed when 3 or 8 equivalents of Ce^{IV} was added. Although the $Ru^V=O$ and Ru^{IV}—O—O—Ru^{IV} intermediates are not found in the last two mass spectra, this does not necessarily indicate their absence. Similarly, only Ru^{III} and Ru^{IV} involved intermediates have been identified for the parent $Ru(bda)(pic)_2$ catalyst through I2M O—O bond formation pathway, indicating the challenge of detecting these intermediate species with high reactivity and low stability by MS [13]. In contrast, a dioxygen intermediate [Ru^{III}—O—O] in the WNA catalytic cycle usually can be tracked under similar *ex-situ* mass spectrometry experiment [57,58]. Overall, the results of *ex-situ* HR ESI-MS investigation support that catalytic water oxidation by Ru-bnda goes through an I2M pathway.

On the basis of the above experimental results, we proposed a typical I2M catalytic cycle for water oxidation by the Ru-bnda catalyst as depicted in Fig. S12. The initial Ru^{II}-bnda is a precatalyst, which is oxidized and coordinates a water to form Ru^{III}—OH_2 as the lowest oxidation state in the catalytic cycle. Ru^{III}—OH_2 is further oxidized to Ru^V=O, which is hydrophobic [44] and displays a radical character, i.e. high spin density on the O atom. Consequently, two molecules of the Ru^V=O (or Ru^{IV}—$O^{\cdot}$) couple with each other in the rate-determining step to form a transient Ru^{IV}—O—O—Ru^{IV} state, which immediately evolves one molecular oxygen, re-coordinates two new H_2O molecules and transforms back to Ru^{III}—OH_2.

DFT calculations were performed to further confirm the I2M mechanism of water oxidation by Ru-bnda. Since the rate-determining step of Ru-bda catalyzed water oxidation reaction is proposed to be the O—O bond formation step in the previous works [15–17], this step with the Ru^V=O species of the complex $Ru(bnda)(pic)_2$ has been researched in detail. We probed free energy profiles of O—O bond formation by modeling the coupling reaction of two Ru^{IV}=$O^{\cdot}$ radical species (Fig. 5). In this pathway the O—O bond formation step is exergonic with a reaction free energy of −4.4 kcal/mol from the pre-reactive dimer to the product dimer, and activation free energy of 8.3 kcal/mol from the pre-reactive dimer to the transition state. The optimal O—O distance at the transition state is 1.92 Å. These findings are in good agreement with $Ru(bda)(pic)_2$ catalyst [11,15,16]. For comparison, we also calculated the WNA pathway for the Ru-bnda, for which an activation free energy of 16.3 kcal/mol was found to be much higher than that of the di-radical coupling reaction, and which is endergonic required a reaction energy of 3.5 kcal/mol. The lower activation free energy of the coupling indicates that the reaction goes through the I2M pathway which is consistent with the results of experimental studies.

4. Discussions

Factors such as seven-coordination configuration, large angle of the O—Ru—O open site and low Ru oxidation potential resulting from the two negative carboxylate groups, have been discussed to explain why Ru-bda catalyst proceeds through the I2M mechanism and is prominently active [15,17,25]. However, the parent Ru-bda, Ru-bnda, Ru-pda, and Ru-biqa catalysts in Fig. 1 have similar first coordination sphere environments, yet these Ru-based catalysts not only show some differences in electrochemical processes but also proceed through different O—O bond formation pathways (Table 1).

These four catalysts may have different Ru^{II}/Ru^{III} redox potentials depending on the backbone structure and substituents, for example, the Ru^{II}/Ru^{III} redox potential of the Ru-bnda is much higher than that of the Ru-bda and Ru-biqa catalysts due to the two electron-withdrawing carboxyl groups at a meta-position of the bda pyridine ring. In contrast, their Ru^{III}/Ru^{IV} and Ru^{IV}/Ru^V couples are found independent of the backbone ligands. Although the Ru-pda showed significantly high potentials for Ru^{II}/Ru^{III} and Ru^{III}/Ru^{IV}, these values cannot be directly applied to compare with other catalysts, because CH_3CN, which may influence the electrochemical performance of Ru-bda based catalysts, was involved in its electrochemical test [35]. The Ru-bnda, Ru-pda, and Ru-biqa catalysts exhibit much lower TONs than the parent Ru-bda, indicating that flexibility of the backbone ligand is very important to the stability of this family of catalysts. The stabilities of the key $[Ru^{IV}$—$OH]^+$ and $[Ru^V$=$O]^+$ intermediates can be influenced by conformational changes in the backbone ligands, including the distortion of the bipyridine backbone and O—Ru—O/N—Ru—N planes [35]. Loss of sufficient rotational flexibility as in the parent Ru-bda catalyst may render the formation of those essential intermediates of the Ru-bnda, Ru-pda, and Ru-biqa energetically demanding. Regarding the O—O bond formation pathway, the Ru-bda and Ru-bnda form O—O bond via I2M, while Ru-pda and Ru-biqa proceed through WNA pathway [35,59]. This indicates that, in addition to the first coordination sphere structure and flexibility of the backbone ligand, there may be more elements that can favor the I2M pathway.

In order to reveal what parameters trigger the switch of O—O bond formation between the WNA and I2M pathways, systematic DFT calculations were carried out on these four catalysts. The

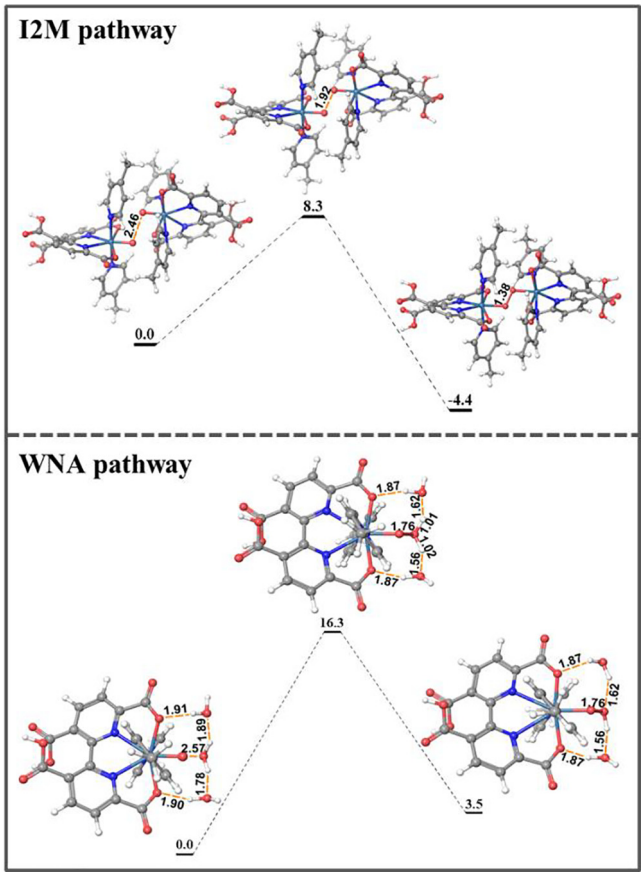


Fig. 5. The calculated relative free energy profile of O—O bond formation of Ru-bnda for the I2M and WNA pathways. The relative Gibbs free energies are given in kcal·mol^{-1} and the bond lengths are given in Å.

theoretical parameters from a DFT calculation that can be considered in the determination of the I2M mechanism are the spin density on the O atom in the Ru^{V}=O state ($O_{RuV=O}$) and the activation free energy of forming the transition [Ru^{V}=O···O=Ru^{V}] dimer [16,17,46,60,61]. Therefore, we focus on the steps related to these two intermediates. The spin density on $O_{RuV=O}$ and activation free energies for the I2M and WNA mechanism of the parent Ru-bda, Ru-bnda, Ru-pda, and Ru-biqa catalysts are summarized in Table 2.

Interestingly, we found that the seven-coordinated Ru^{V}=O states of these four catalysts not only have similarly high spin density on the $O_{RuV=O}$ atom but also similar conformation with approximate bond lengths and angles (Fig. 6a and Table 2), indicating that high spin density on the $O_{RuV=O}$ atom may be a necessary but not sufficient condition to determine the adoption of the I2M mechanism during catalysis. The activation free energy for the formation of the transition [Ru^{V}=O···O=Ru^{V}] dimer from the pre-reactive states showed the I2M pathway would be more favorable for all four catalysts without considering other potential factors.

These observations are consistent with previous reports showing that formation of the pre-reactive state from two solvated Ru^{V}=O monomers is the sole determining factor for the efficiency of Ru-bda catalysts [60–62]. Yan et al. also emphasized that, for a bimolecular reaction, the major contributor to the overall reaction barrier is the entropic term, a point that is intuitive but often overlooked nonetheless [30]. Accordingly, the O—O bond formation pathway of a Ru-bda derived catalyst is determined not only by the nature of its $O_{RuV=O}$ but also other factors. We hypothesize that O—O bond formation might be influenced by the whole

Table 2
Calculated spin density on $O_{RuV=O}$, and activation free energies (kcal mol^{-1}) of the O—O bond formation for the I2M and WNA mechanism of the parent Ru-bda, Ru-bnda, Ru-pda, and Ru-biqa catalysts.

Catalysts	Spin density of $O_{RuV=O}$	$\Delta G^{\neq}_{(I2M)}$ (kcal mol^{-1})	$\Delta G^{\neq}_{(WNA)}$ (kcal mol^{-1})
Ru-bda	0.72225	6.9	20.6
Ru-bnda	0.72286	8.3	16.3
Ru-pda	0.71141	6.2	20.6
Ru-biqa	0.72594	6.9	20.0

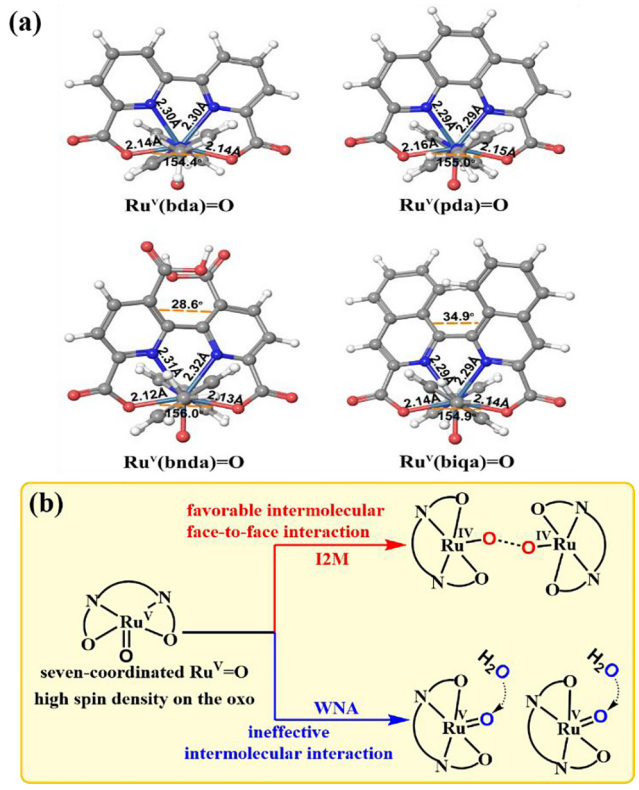


Fig. 6. (a) DFT-optimized structure of the [Ru^{V}(bda)=O], [Ru^{V}(pda)=O], [Ru^{V}(bnda)=O] and [Ru^{V}(biqa)=O]. (b) Two alternative reaction pathways for seven-coordinated Ru^{V}=O species depending on the nature of the catalyst backbone.

coordination environment and the resulting changes in intermolecular interaction in aqueous solution (Fig. 6b).

5. Conclusions

This work presents the synthesis and catalytic water oxidation properties of a Ru-bnda catalyst with steric hindrance and hydrophilicity on the backbone. The experimental results and DFT calculations confirmed that the Ru-bnda catalyst goes through the I2M mechanism during water-oxidation catalysis with an initial rate of 10 s^{-1}. To make a comprehensive comparison, we carried out DFT calculations on the Ru-pda, parent Ru-bda, Ru-bnda, and Ru-biqa catalysts. According to the spin density on $O_{RuV=O}$ and the activation free energy for the formation of the transition [Ru^{V}=O···O=Ru^{V}] dimer from the pre-reactive states, the I2M pathway would be more favorable for all four catalysts. However, this is inconsistent with the experimental observations. To solve this contravention, the solvation effect and the step of colliding two Ru^{V}=O species need to be considered in the DFT calculations. These findings offer a cogent guidance for further understanding the catalytic mechanisms of the Ru-bda series catalysts. More

comprehensive experimental studies and theoretical calculations are in progress to further reveal these observations.

Declaration of Competing Interest

The authors declare that they have no known competing financial interests or personal relationships that could have appeared to influence the work reported in this paper.

Acknowledgments

The authors acknowledge the financial support from the Swedish Research Council (2017-00935), Swedish Energy Agency, the Knut and Alice Wallenberg Foundation, the National Natural Science Foundation of China (21120102036), the National Basic Research Program of China (973 program, 2014CB239402), and the China Scholarship Council (CSC). All calculations were performed on resources provided by the Swedish National Infrastructure for Uppsala Multidisciplinary Center for Advanced Computational Science (UPPMAX) under the project number SNIC2017-1-339 and the National Supercomputing Center in Linköping, Sweden.

Appendix A. Supplementary data

Supplementary data to this article can be found online at https://doi.org/10.1016/j.jechem.2020.06.036.

References

[1] N.S. Lewis, D.G. Nocera, Proc. Natl. Acad. Sci. U. S. A. 103 (2006) 15729–15735.
[2] B. Zhang, L. Sun, Chem. Soc. Rev. 48 (2019) 2216–2264.
[3] P. Garrido-Barros, C. Gimbert-Suriñach, R. Matheu, X. Sala, A. Llobet, Chem. Soc. Rev. 46 (2017) 6088–6098.
[4] M.D. Kärkäs, O. Verho, E.V. Johnston, B. Åkermark, Chem. Rev. 114 (2014) 11863–11871.
[5] R. Matheu, M.Z. Ertem, C. Gimbert-Surinach, X. Sala, A. Llobet, Chem. Rev. 119 (2019) 3453–3471.
[6] R. Matheu, P. Garrido-Barros, M. Gil-Sepulcre, M.Z. Ertem, X. Sala, C. Gimbert-Suriñach, A. Llobet, Nat. Rev. Chem. 3 (2019) 331–341.
[7] S.W. Gersten, G.J. Samuels, T.J. Meyer, J. Am. Chem. Soc. 104 (1982) 4029–4030.
[8] J. Shi, Y.H. Guo, F. Xie, Q.F. Chen, M.T. Zhang, Angew. Chem. Int. Ed. 59 (2020) 4000–4008.
[9] C. Sens, I. Romero, M. Rodríguez, A. Llobet, T. Parella, J. Benet-Buchholz, J. Am. Chem. Soc. 126 (2004) 7798–7799.
[10] R. Zong, R.P. Thummel, J. Am. Chem. Soc. 127 (2005) 12802–12803.
[11] L. Duan, F. Bozoglian, S. Mandal, B. Stewart, T. Privalov, A. Llobet, L. Sun, Nat. Chem. 4 (2012) 418–423.
[12] B. Zhang, L. Sun, J. Am. Chem. Soc. 141 (2019) 5565–5580.
[13] L. Duan, A. Fischer, Y. Xu, L. Sun, J. Am. Chem. Soc. 131 (2009) 10397–10399.
[14] L. Wang, L. Duan, Y. Wang, M.S.G. Ahlquist, L. Sun, Chem. Commun. 50 (2014) 12947–12950.
[15] L. Duan, C.M. Araujob, M.S.G. Ahlquist, L. Sun, Proc. Natl. Acad. Sci. U. S. A. 109 (2012) 15584–15588.
[16] J. Nyhlén, L. Duan, B. Åkermark, L. Sun, T. Privalov, Angew. Chem. Int. Ed. 49 (2010) 1773–1777.
[17] L. Wang, L. Duan, B. Stewart, M. Pu, J. Liu, T. Privalov, L. Sun, J. Am. Chem. Soc. 134 (2012) 18868–18880.
[18] T. Liu, B. Zhang, L. Sun, Chem. Asian J. 14 (2019) 31–43.
[19] M.D. Karkas, B. Akermark, Dalton Trans. 45 (2016) 14421–14461.
[20] H.Y. Du, S.C. Chen, X.J. Su, L. Jiao, M.T. Zhang, J. Am. Chem. Soc. 140 (2018) 1557–1565.
[21] P. Garrido-Barros, S. Grau, S. Drouet, J. Benet-Buchholz, C. Gimbert-Suriñach, A. Llobet, ACS Catal. 9 (2019) 3936–3945.
[22] P. Garrido-Barros, I. Funes-Ardoiz, S. Drouet, J. Benet-Buchholz, F. Maseras, A. Llobet, J. Am. Chem. Soc. 137 (2015) 6758–6761.
[23] S.M. Barnett, K.I. Goldberg, J.M. Mayer, Nat. Chem. 4 (2012) 498–502.
[24] J.L. Fillol, Z. Codola, I. Garcia-Bosch, L. Gomez, J.J. Pla, M. Costas, Nat. Chem. 3 (2011) 807–813.
[25] L. Duan, L. Wang, F. Li, F. Li, L. Sun, Acc. Chem. Res. 48 (2015) 2084–2096.
[26] B. Zhang, F. Li, R. Zhang, C. Ma, L. Chen, L. Sun, Chem. Commun. 52 (2016) 8619–8622.
[27] Y. Jiang, F. Li, F. Huang, B. Zhang, L. Sun, Chin. J. Catal. 34 (2013) 1489–1495.
[28] Y. Sato, S.-Y. Takizawa, S. Murata, Eur. J. Inorg. Chem. 2015 (2015) 5495–5502.
[29] L. Duan, L. Wang, A.K. Inge, A. Fischer, X. Zou, L. Sun, Inorg. Chem. 52 (2013) 7844–7852.
[30] Y. Xie, D.W. Shaffer, J.J. Concepcion, Inorg. Chem. 57 (2018) 10533–10542.
[31] Z. Liu, Y. Gao, Z. Yu, M. Zhang, J. Liu, Chin. J. Catal. 36 (2015) 1742–1749.
[32] D.W. Shaffer, Y. Xie, D.J. Szalda, J.J. Concepcion, Inorg. Chem. 55 (2016) 12024–12035.
[33] Q. Daniel, L. Duan, B.J.J. Timmer, H. Chen, X. Luo, R. Ambre, Y. Wang, B. Zhang, P. Zhang, L. Wang, F. Li, J. Sun, M.S.G. Ahlquist, L. Sun, ACS Catal. 8 (2018) 4375–4382.
[34] L. Duan, Y. Xu, M. Gorlov, L. Tong, S. Andersson, L. Sun, Chem. Eur. J. 16 (2010) 4659–4668.
[35] L. Tong, L. Duan, Y. Xu, T. Privalov, L. Sun, Angew. Chem. Int. Ed. 50 (2011) 445–449.
[36] R. Matheu, M.Z. Ertem, J. Benet-Buchholz, E. Coronado, V.S. Batista, X. Sala, A. Llobet, J. Am. Chem. Soc. 137 (2015) 10786–10795.
[37] R. Matheu, M.Z. Ertem, C. Gimbert-Suriñach, J. Benet-Buchholz, X. Sala, A. Llobet, ACS Catal. 7 (2017) 6525–6532.
[38] N. Govindarajan, A. Tiwari, B. Ensing, E.J. Meijer, Inorg. Chem. 57 (2018) 13063–13066.
[39] Z. Chen, J.J. Concepcion, J.W. Jurss, T.J. Meyer, J. Am. Chem. Soc. 131 (2009) 15580–15581.
[40] J.J. Concepcion, M.-K. Tsai, J.T. Muckerman, T.J. Meyer, J. Am. Chem. Soc. 132 (2010) 1545–1557.
[41] N. Govindarajan, E.J. Meijer, Inorganics 7 (2019) 62.
[42] J.M. Kamdar, D.C. Marelius, C.E. Moore, A.L. Rheingold, D.K. Smith, D.B. Grotjahn, ChemCatChem 8 (2016) 3045–3049.
[43] Y. Xie, D.W. Shaffer, A. Lewandowska-Andralojc, D.J. Szalda, J.J. Concepcion, Angew. Chem. Int. Ed. 55 (2016) 8067–8071.
[44] D.W. Shaffer, Y. Xie, D.J. Szalda, J.J. Concepcion, J. Am. Chem. Soc. 139 (2017) 15347–15355.
[45] J. Yang, J. An, L. Tong, B. Long, T. Fan, L. Duan, Inorg. Chem. 58 (2019) 3137–3144.
[46] T. Fan, L. Duan, P. Huang, H. Chen, Q. Daniel, M.S.G. Ahlquist, L. Sun, ACS Catal. 7 (2017) 2956–2966.
[47] F. Yu, D. Poole 3rd, S. Mathew, N. Yan, J. Hessels, N. Orth, I. Ivanović-Burmazović, J.N.H. Reek, Angew. Chem. Int. Ed. 57 (2018) 11247–11251.
[48] M. Schulze, V. Kunz, P.D. Frischmann, F. Wurthner, Nat. Chem. 8 (2016) 576–583.
[49] E.M. Nagy, A. Pettenuzzo, G. Boscutti, L. Marchio, L. Dalla Via, D. Fregona, Chem. Eur. J. 18 (2012) 14464–14472.
[50] U. Dawid, F.P. Pruchnik, R. Starosta, Dalton Trans. (2009) 3348–3353.
[51] G.M. Sheldrick, Acta Cryst. A 64 (2008) 112–122.
[52] A.D. Bochevarov, E. Harder, T.F. Hughes, J.R. Greenwood, D.A. Braden, D.M. Philipp, D. Rinaldo, M.D. Halls, J. Zhang, R.A. Friesner, Int. J. Quantum Chem. 113 (2013) 2110–2142.
[53] Y. Zhao, D.G. Truhlar, Theor. Chem. Acc. 120 (2008) 215–241.
[54] L. Goerigk, S. Grimme, Phys. Chem. Chem. Phys. 13 (2011) 6670–6688.
[55] S. Grimme, J. Antony, S. Ehrlich, H. Krieg, J. Chem. Phys. 132 (2010) 154104.
[56] P.J. Hay, W.R. Wadt, J. Chem. Phys. 82 (1985) 299–310.
[57] L. Tong, A.K. Inge, L. Duan, L. Wang, X. Zou, L. Sun, Inorg. Chem. 52 (2013) 2505–2518.
[58] D.J. Wasylenko, C. Ganesamoorthy, M.A. Henderson, B.D. Koivisto, H.D. Osthoff, C.P. Berlinguette, J. Am. Chem. Soc. 132 (2010) 16094–16106.
[59] D. Scherrer, M. Schilling, S. Luber, T. Fox, B. Spingler, R. Alberto, C.J. Richmond, Dalton Trans. 45 (2016) 19361–19367.
[60] S. Zhan, D. Mårtensson, M. Purg, S.C.L. Kamerlin, M.S.G. Ahlquist, Angew. Chem. Int. Ed. 56 (2017) 6962–6965.
[61] T. Fan, S. Zhan, M.S.G. Ahlquist, ACS Catal. 6 (2016) 8308–8312.
[62] S. Zhan, R. Zou, M.S.G. Ahlquist, ACS Catal. 8 (2018) 8642–8648.